Article

Generalized, Complete and Accurate Modeling of Non-Ideal Push–Pull Converters for Power System Analysis and Control

Francisco José Vivas * , **Francisca Segura** and **José Manuel Andújar**

Centre for Research on Technology, Energy and Sustainability, University of Huelva, 21071 Huelva, Spain; francisca.segura@diesia.uhu.es (F.S.); andujar@diesia.uhu.es (J.M.A.)
* Correspondence: francisco.vivas@diesia.uhu.es

Abstract: Power converters are a basic element for the control and design of any power electronic system. Among the many available topologies, the push–pull converter is widely used due to its versatility, safety and efficiency. For its correct analysis, sizing, simulation and control, models that meet the characteristics of generality, accuracy and simplicity are required, especially if its control is to be optimized by means of some analytical technique. This requires models that consider the practical non-idealities intrinsic to the converter, as well as being intuitive and easy to handle analytically in a control loop. In general, the models reviewed in the scientific literature adopt simplifications in their definition that are detrimental to their accuracy. In response to the posed problem, this work presents a generalized, complete, accurate and versatile model of real (non-ideal) push–pull converters, ideal for the analysis, simulation, and control of power systems. Following the premise of general and complete converters, the proposed model includes all the practical non-idealities of the converter elements, and it is accurate because it faithfully reflects its dynamics. Furthermore, the model is versatile, as its state space formulation allows for its easy adaptability to the converter operating conditions (voltage, current and temperature) for each sampling time. Also, the model is excellent for use in model-based control techniques, as well as for making very accurate simulators. The behavior of the developed model has been contrasted with a real push–pull converter, as well as with reference models present in the scientific literature for both dynamic and steady-state response tests. The results show excellent performance in all the studied cases, with behavior faithful to the real converter and with relative errors that are much lower than those obtained for the reference models. It follows that the model behaves like a digital twin of a real push–pull converter.

Keywords: state-space model; isolated DC/DC converter; modeling; push–pull converter; model-based controller

1. Introduction

Power converters are one of the standard components of power electronic systems, since they allow for the integration and control of the different blocks that determine their architecture [1,2].

The field of application of power converters and, in particular, DC/DC converters, is huge [3,4]. Thus, for example, in power grids, especially in renewables ones, DC/DC power converters connect the generators to the buses, so they are the elements that allow for the coupling of both impedances to deliver regulated power to the buses [5,6].

Currently, there are multiple power converter topologies, and among them, the push–pull topology stands out as one of the most widely used in the design of switched-mode power supplies, and DC/DC converters and power inverters, forming fundamental pillars for the definition of the architecture and control of power systems [7,8]. In particular, the push–pull topology is becoming of great interest for the design and control of power systems in applications as diverse as electric vehicles [9], energy conversion in renewable microgrids [7], high-voltage direct-current (HVDC) transmission lines [10] and the

integration and control of energy storage systems based on batteries or hydrogen technologies [11]. This is due to several factors, including the following: its simplicity, due to the reduced number of switching devices [12]; its versatility, as the use of a high-frequency (HF) transformer allows for the design of buck or boost topologies without restrictions in the conversion ratio or modifications in the topology [13]; its scalability, as its operating power can vary from a few watts to hundreds of kW [14]; and its excellent performance compared to other isolated topologies [14]. Among other reasons, these contribute to the interest in the study of this topology.

For the correct design, simulation, implementation and control of push–pull converters in real applications, it is very useful to have analytical models whose behavior is as close as possible to that of the real converter [15,16]. This, among other things, allows for studies to improve the converter's performance, as well as the prediction and analysis of its dynamic and stationary responses depending on the application.

A good converter model, regardless of its formulation, must combine accuracy and modularity and, at the same time, guarantee the practical computability required for the design of real-time controllers. Therefore, according to these requirements, it is fundamental that a push-pull converter model that is considered general and complete considers all its practical non-idealities. In addition, its formulation must, on the one hand, facilitate its fast computation, and, on the other hand, be able to adapt to the variations in the non-idealities depending on the operating conditions of the converter. These premises comprise the starting point for this research.

Depending on the non-idealities that are considered and the adopted simplifications, the modeling solutions found in the literature are diverse in terms of complexity and purpose. To facilitate their study and highlight the contributions of this research, the models studied in the scientific literature have been grouped according to the considered parameters, using the following classification.

First, the simplest and most widespread solutions, called type 1 models (T1M), are based on the ideal model of the HF transformer and all switching devices (transistors and diodes). Depending on the model, losses associated with the inductance and the filter capacitor (Figure 1) can be considered. This allows, by applying the converter transformation ratio, for the proposal of a simplified circuit with respect to the transformer secondary, with behavior, architecture, and model resembling that of an equivalent buck converter.
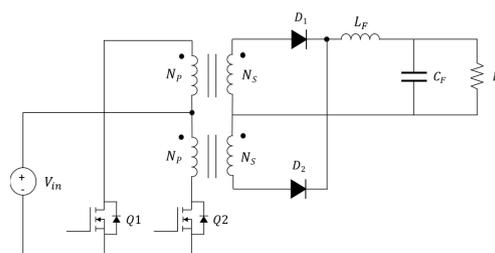

Figure 1. Ideal circuit of the push–pull converter.

These models have been successfully used in multiple applications with different formulations. Thus, [10] and [17] show, respectively, state-space models that are oriented to the control of fuel cell systems in DC microgrids and auxiliary starting systems for electric vehicles. Similar models, formulated as impedance models, are used for the control and design of converters in DC power systems for the integration of electrolyzers in renewable grids [17], and the design of modular multilevel converters for high-voltage applications [10]. Finally, a more complete converter model for photovoltaic microinverter control is described in [7]. This model is based on the small-signal model of the converter, formulated as a transfer function, and integrates the non-idealities associated with the output filter.

The use of T1M may be a good starting point for the preliminary design of the converter and its control loops, but often leads to considerable discrepancies with actual behavior.

This is mainly due to the strong influence of the converter's non-idealities with respect to its operating conditions, power and switching frequency [18].

Secondly, type 2 models (T2M) are those that consider some non-idealities in the HF transformer (leakage resistances and inductances of the primary and secondary windings) and, depending on the work, they also consider some non-idealities in the switching devices and in the filter inductance and capacitor. An example of such models is developed in [19]. Specifically, this model is formulated in state-space representation, and is a control-oriented average model of bi-directional dual active bridge converters for use in solid-state transformers, smart grids, and electric/hybrid vehicle applications. It is a simplified model that integrates the effect of the resistance and inductances of the HF transformer windings, and the series resistance of the output filter components. Refs. [20,21] present a model formulated as a transfer function for the analysis and control of push–pull converters. In particular, Ref. [20] models a bidirectional pulse-width modulation (PWM) plus phase-shift-modulated push–pull converter, while [21] models a classical topology converter for use in isolated high-voltage applications. Again, these models are highly simplified, as they only integrate the non-idealities associated with the HF transformer windings.

Finally, a more complete model for the sizing and control of bidirectional converters is developed in [22]. This model is formulated as an average and small-signal state-space model, and integrates non-idealities of the HF transformer, such as winding inductance and magnetization losses. Despite the improvement in T2M compared to T1M, none of the reviewed works presents a complete solution that models all the non-idealities (at least all the practical ones) of the converter. In particular, as far as the HF transformer is concerned, the parasitic capacitances of its windings, which can have a considerable effect on the dynamic response of the model depending on the switching frequency and the winding technique used, are ignored [23]. Furthermore, the non-idealities associated with the switching devices are also not considered.

Finally, type 3 models (T3M) encompass the most complex and complete models found in the literature. These models consider an important part of the non-idealities of both the HF transformer and the rest of the fundamental components of the converter. Such models are scarce in the literature; however, some recent examples can be found. Thus, Ref. [24] presents the analysis and modeling of a voltage-compensated push–pull converter. In this case, the model includes non-idealities associated with the HF transformer, specifically its magnetization inductance, as well as non-idealities of the electronic switches, namely its output capacitances. It is a control-oriented model represented in the form of a transfer function, where simplicity is paramount, and whose formulation is based on the small-signal model of the converter. On the other hand, Ref. [23] presents a very complete model applied to the control of three-phase push-pull converters. This model is also formulated as a transfer function, and integrates the non-idealities associated with the magnetizing inductance of the HF transformer, the internal resistance of certain passive components and electronic switches, and the rectifier diodes.

The improvements brought by these models are noticeable, as they consider some non-idealities of the classical model of the real transformer (Figure 2), as well as the parasitic output capacitor of the transistors (Figure 3). However, the complete modelling of the converter, with particular attention to all the practical non-idealities associated with the HF transformer, remains to be addressed.

From the analysis of the scientific literature review, it is concluded that, despite the large number of applications and published works, no analytical mathematical model has been found that integrates all the practical non-idealities of the push–pull converter. The main problem of the analyzed models, including the few T3M models found, lies in the deviations between theoretical and experimental behavior outside specific operating conditions, since the push–pull converter is a strongly non-ideal system [25]. This implies that the models presented in the literature are not completely general, regardless of the converter power and operating conditions.
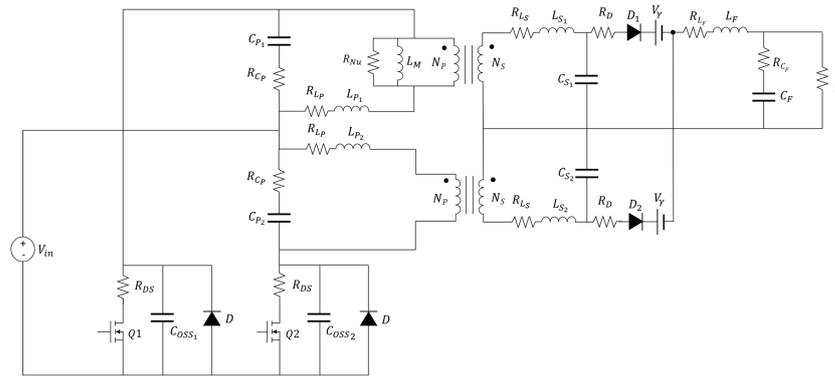
Figure 2. Non-ideal (actual) circuit reduced to the secondary of the push–pull converter in Figure 1.
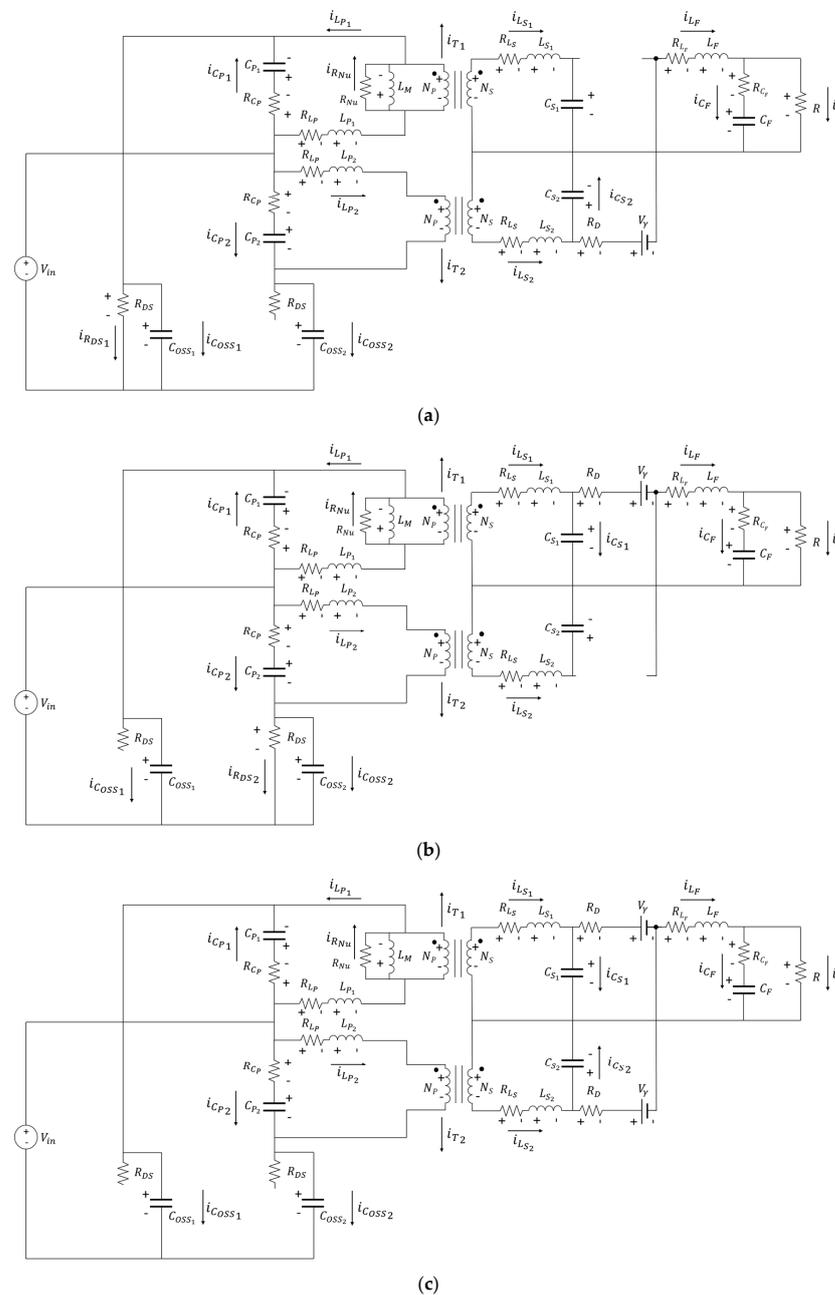
Figure 3. (**a**) Equivalent circuit reduced to the secondary for case 1; (**b**) for 2; and (**c**) for 3.

This analysis leads to the conclusion that there is a clear need for a general, accurate, fully interpretable, and practical model of push–pull converters to serve as a tool for the design and testing of high-performance model-based controllers for power system management, advanced analysis, precision simulations and digital twins. This is precisely the objective of this work and its main novelty.

Although the procedure used to o build the developed model is well known, since it is based on Kirchhoff's laws and a standard averaging method, the main contribution of this work, in the authors' opinion, is the development of the most general and complete model published to date (at least to the authors' knowledge). To summarize the contributions of this research, the novelties of the proposed model are listed below:

- A control-oriented linear parameter-variable state space (LPV) model is presented.
- The model is general, simple, and accurate. To achieve this, it considers, in a very intuitive way, the main non-idealities of the converter associated with the HF transformer, electronic switches, diodes, and passive components.
- The model is fully discrete and linear each time, at each sampling period, which implies that a different transfer function can be generated at each sampling period. However, perhaps more important is that, if the sampling period is small enough, the model perfectly captures the nonlinear dynamics of the converter over time.
- Its direct formulation in a state space from a first-order differential equation in each energy storage element allows for the development of a very high-order model (a transfer function model that was mathematically developed in the usual way would require a differential equation of order 13), which is necessary to consider the high number of non-idealities of the converter. In any case, using the developed state model, it is very easy to obtain an impedance or transfer function model for each sampling period; this is sufficient to solve the linear state equation each time. Regarding the latter, although the procedure used to obtain transfer functions from linear state models is straightforward, there is no guarantee that an output–input relationship can always be found, especially in complex and very high-order models such as this one.
- Although it is able to accurately track the nonlinear behavior of the converter, the model provides modularity and allows for the application of (well-known and highly experienced) linear control theories at a low computational cost [26].
- Unlike impedance or transfer function models, the developed model explicitly integrates as state variables (impedance or transfer function models only deal with input–output relationships) the main electrical variables associated with the converter's non-idealities. This allows for the effect and impact of non-idealities on the dynamic response of the converter to be evaluated individually. It is general and flexible, and can easily be adapted to consider variations in the values of the converter's non-idealities (linear or non-linear), such as the variation in the magnetizing inductance, the dependence of certain parameters on temperature, etc. Finally, the impedance or transfer function models are lineal all the time, from the initial condition to steady state, if this is reached. Moreover, this is the only time information that they contain. This is not the case with the developed model, which constantly adapts (at each sampling period) its operation to accurately follow the nonlinear behavior of the real converter, while also providing explicit time information all the time.

To highlight the novelty of this research, Table 1 summarizes its main characteristics in comparison with the analyzed literature.

The rest of this article is organized as follows. Section 2 studies the operating modes of the converter and develops its dynamic equations to obtain the average and small-signal model expressions. In Section 3, an experimental validation of the developed model is carried out, together with a comparison with the most complete models (used as a reference) found in the literature. The results are discussed in Section 4. Finally, Section 5 concludes the paper by discussing future work.

Table 1. Summary of push–pull converter modelling solutions found in the literature compared to the authors' proposal.

Reference	Non-Idealities Considered				Formulation	Design Objective
	HF Transformer	Electronic Switches	Rectifier Diodes	Output LC Filter		
[11,27]	-	-	-	-	Average state-space model	Control-oriented design
[10,17]	-	-	-	-	Impedance model	Control-oriented design, sizing
[7]	-	-	-	Int. resistance	Transfer function	Control-oriented design
[19]	Int. resistance of windings Leakage inductance of windings	-	-	Int. resistance	Average state-space model	Control-oriented design
[20,21]	Leakage inductance of windings	-	-	-	Transfer function	Control-oriented design, advanced analytics
[22]	Int. resistance of windings Leakage inductance of windings Core losses	-	-	-	Average and small signal state-space model	Control-oriented design, sizing
[23]	Leakage inductance of windings Core magnetization inductance	Out. capacitance	-	-	Transfer function	Control-oriented design
[24]	Int. resistance of windings Core magnetization inductance	Drain-sink resistance	Forward voltage	Int. resistance	Transfer function	Control-oriented design
Authors proposal	Int. resistance of windings Leakage inductance of windings Parasitic capacitances of windings Core magnetization inductance Core losses	Out. capacitance Drain-sink resistance	Int. resistance Forward voltage	Int. resistance	Average and small-signal discrete state-space model	Control-oriented design, advanced analytics and digital twins

2. Modeling

This section develops the methodology used to for obtain the dynamic model of the converter. To do this, firstly and for simplicity, the operating principle of the push–pull converter based on the ideal model will be described. This operating principle is similar to that of the non-ideal converter, and is defined by the operation of the electronic switches during a control signal period.

Next, before entering the modelling step, the criteria considered in the definition of the model will be described, in short, the non-idealities, assumptions and simplifications to be considered.

Finally, the average and small-signal state-space model of the converter will be developed. To obtain this, the equivalent circuits will be analyzed for each of the three cases, defined according to the operating principle.

2.1. Operating Principle

The push–pull converter, like all other power converters, owes its operation to the controlled flow of current through its circuit. This is accomplished by the controlled switching of its electronic switches and energy storage in its inductors and capacitors. The ideal circuit model is shown in Figure 1.

Based on the ideal circuit model (Figure 1), its operating principle will be explained on the basis of three operating modes, depending on whether the electronic switches (Mosfets) are in conduction or cut-off (case 1: Q_1 ON and Q_2 OFF, case 2: Q_1 OFF and Q_2 *ON*, ON and Case 3: Q_1 and Q_2 OFF). In cases 1 or 2, current flows through the corresponding transformer primary winding (see Figure 1), magnetizing its transformer core. The voltage induced in the secondary (the polarity correspondence between the primary and the secondary is given by the dots of the respective windings; see Figure 1) will drive diode

D_1 or D_2, with one of the branches always being active (see Figure 1). The current of each active branch will flow through the L_F-C_F circuit and supply the load R. In case 3, there is no current through the primary windings and, therefore, no voltage induction in the secondary. Since the inductor current is continuous, it follows that the energy stored in L_F, like that stored in C_F, is also continuous, so D_1 and D_2 conduct.

2.2. Non-Ideal Equivalent Circuit Model

The circuit in Figure 1 is only a simple approximation of the real operation of the practical push–pull converter, so an accurate model will require consideration of the non-idealities of the real push–pull converter. Thus, it is necessary to have a complete model, which integrates the non-idealities of the converter while combining the characteristics of accuracy and simplicity.

Considering the non-idealities of the push–pull converter, which can be innumerable, it is necessary to limit their number to those that have a real influence in practice. In addition, unpredictable non-idealities, such as those due to poor converter design and construction, must be avoided, for example the type of connections used, the design of the printed circuit board, the wiring, the design of the gate-driver circuits, poor sizing and construction of the HF transformer, and the use of poor-quality components.

In view of the above, to consider an approachable modelling problem, it is necessary to ensure that the converter has been designed and built correctly and that its components are of professional quality. All the considered non-idealities and assumptions used in the modeling will be described below.

For the modelling of the HF transformer, the well-known non-ideal transformer model T with parameters reduced to the secondary will be used. Then, to set up the practical circuit, and based on the practical principle being described, it is considered that the transformer is well designed, which makes it possible to assume that the transformer will be fully magnetized and demagnetized in each operating cycle, its core will always operate within the linear region of the magnetization curve, and its parameters will be identical for each winding. In addition, the parasitic inductances and resistances associated with the power loop, wiring and connectors will not be considered, since the casuistry can be enormous as these parameters depend on the design and physical implementation of the converter. In any case, these parameters are relatively easy to minimize with good converter design and manufacturing.

The non-idealities considered for power switching devices are series drain-sink saturation resistance and parallel output capacitances for Mosfets, direct resistance, and the corresponding threshold voltage for rectifier diodes. Switching losses have not been considered in this analysis for several reasons. The first is that these losses are influenced by parameters external to the converter, which are difficult to control or know, such as the output voltage or resistance of the gate driver circuit of the power transistors. This leads to the second reason: the limitations of the complexity of the model. The consideration of switching losses would add further complexity to the already high order of the model. Moreover, considering as the article considers the switching devices to be of good quality, and as the switching times are much lower than the conduction times, losses can be considered negligible.

For diodes and electronic switches, the characteristics and non-idealities associated with devices of the same model and manufacturer shall be considered identical. On the other hand, it is known that there are strong non-linear relationships in the diode with respect to its threshold voltage and, in the case of electronic switches, with respect to the drain-sink voltage (output capacitance) and the influence of temperature on the drain-sink resistance. However, to ensure that the analysis is not unnecessarily complex and there is no loss of generality, constant parameters will be taken, which are linked to the current operating conditions of voltage, current and temperature electronic switches at a given sampling time.

Accordingly, the model can easily be adapted to the specific operating conditions at each sampling time. For this purpose, a recursive linearization process can be carried out to obtain the best approximation of the value of each parameter, depending on the operating point for each sampling period. Therefore, the developed model is valid and general, and to update it, it is sufficient to modify the linearized parameter to define an LPV model for each sampling period [28]. This allows for the design of model-based adaptive controllers [29].

Finally, as usual, the maximum switching frequency of the switching devices will be much higher than that corresponding to the operating frequency of the converter. Likewise, assuming, as already mentioned in this section, that components are of professional quality, their leakage currents can be neglected.

Thus, the non-idealities considered in the modeling of the non-ideal push–pull converter are listed below:

For the transformer, series resistances and leakage inductances, and the capacitances of the primary and secondary windings (R_{L_P}, R_{L_S}, $L_{P_{1,2}}$, $L_{S_{1,2}}$, $C_{P_{1,2}}$ and $C_{S_{1,2}}$, respectively), as well as transformer core losses associated with magnetization current, eddy currents and parasitic fluxes (L_M and R_{Nu}), were considered. In this case, the parameters of the parallel branch of the transformer model were concentrated in the upper primary winding.

For the power-switching devices, the series drain-sink saturation resistances (R_{DS}) and parallel output capacitances ($C_{OSS_{1,2}}$) of the transistors, as well as the conducting resistance (R_D) and the corresponding threshold voltage (V_γ) of the rectifier diodes, were considered.

Finally, for the converter output LC filter, the series resistance of both the inductance (R_{L_F}) and the filter capacitor (R_{C_F}) were considered. Please see "Nomenclature" for the meaning of each parameter.

Based on this, Figure 2 shows the complete non-ideal equivalent model reduced to the secondary of the push–pull converter in Figure 1.

2.3. Modeling

In this section, the general formulation used to obtain the average and small-signal state-space models of the push–pull converter is developed. Considering the criteria of generality and accuracy, the model integrates all the practical non-idealities of the converter. As for the state vector, as usual, it is formed by the currents or voltages in the energy storage elements, many of them inductances or parasitic capacitances, respectively. Also, from a controller design perspective, the model outputs integrate the main converter variables that are to be controlled, i.e., output voltage and current, which are also measurable. Regarding model inputs, the average developed model includes the converter input voltage as the input variable (single input–multiple output (SIMO) model), while the small-signal model also includes the duty cycle (multiple input–multiple output (MIMO) model).

Finally, for their determination, the differential equations governing the converter dynamics are defined using classical circuit theory, applying mesh analysis based on Kirchhoff's voltage and current laws.

As previously mentioned, to obtain the dynamical model, the behavior of the push–pull converter will be analyzed based on the operation of its electronic switches. Thus, for the three modes of operation, cases 1–3, the equivalent circuits of Figures 2 and 3a–c, respectively, are obtained. From here, for cases 1–3, the state variables (1)–(8) are obtained.

$$v_{L_{P_1}}(t) = L_{P_1}\frac{di_{L_{P_1}}(t)}{dt} = -i_{L_{P_1}}(t){\cdot}R_{L_P} + i_{C_{P_1}}(t){\cdot}R_{C_P} + v_{C_{P1}}(t) - i_{R_{Nu}}(t){\cdot}R_{Nu} \tag{1}$$

$$v_{L_{P_2}}(t) = L_{P_2}\frac{di_{L_{P_2}}(t)}{dt} = -i_{L_{P_2}}(t){\cdot}R_{L_P} + i_{C_{P_2}}(t){\cdot}R_{C_P} + v_{C_{P2}}(t) + i_{R_{Nu}}(t){\cdot}R_{Nu} \tag{2}$$

$$v_{L_M}(t) = L_M\frac{di_{L_M}(t)}{dt} = i_{R_{Nu}}(t){\cdot}R_{Nu} \tag{3}$$

$$v_{L_{S_1}}(t) = L_{S_1}\frac{di_{L_{S_1}}(t)}{dt} = -i_{L_{S_1}}(t){\cdot}R_{L_S} - N{\cdot}i_{R_{Nu}}(t){\cdot}R_{Nu} - v_{C_{S_1}}(t) \tag{4}$$

$$v_{L_{S_2}}(t) = L_{S_2}\frac{di_{L_{S_2}}(t)}{dt} = -i_{L_{S_2}}(t)\cdot R_{LS} + N\cdot i_{R_{Nu}}(t)\cdot R_{Nu} - v_{C_{S_2}}(t) \tag{5}$$

$$i_{C_{P1}}(t) = C_{P_1}\frac{dv_{Cp1}(t)}{dt} = \frac{v_{in}(t)}{R_{C_P}} - \frac{v_{C_{OSS}1}(t)}{R_{C_P}} - \frac{v_{C_{P_1}}(t)}{R_{C_P}} \tag{6}$$

$$i_{C_{P2}}(t) = C_{P_2}\frac{dv_{Cp2}(t)}{dt} = \frac{v_{in}(t)}{R_{C_P}} - \frac{v_{C_{OSS}2}(t)}{R_{C_P}} - \frac{v_{C_{P_2}}(t)}{R_{C_P}} \tag{7}$$

$$i_{C_F}(t) = C_F\frac{dv_{C_F}(t)}{dt} = i_{L_F}(t) - i_R(t) \tag{8}$$

where $N = N_s/N_p$, and $i_{R_{Nu}}$ is given by (9):

$$i_{R_{Nu}}(t) = i_{L_{P_1}}(t) - i_{L_M}(t) - i_{T_1}(t) \tag{9}$$

By following any of Figure 3, currents i_{T_1} and i_{T_2} in the transformer are given, respectively, by (10) and (11).

$$i_{T_1}(t) = i_{T_2}(t) + \left(-i_{L_{S_1}}(t) + i_{L_{S2}}(t)\right)N \tag{10}$$

$$i_{T_2}(t) = i_{L_{P_2}}(t) \tag{11}$$

The converter output current (i_R) is calculated from the converter output voltage (v_R) and the load resistance (R) as (12).

$$i_R(t) = \frac{v_R(t)}{R} = \frac{i_{CF}(t)\cdot R_{C_F} + v_{C_F}(t)}{R} \tag{12}$$

In the same way, the rest of the state variables can be obtained, now particularized for each operating mode. Thus, for case 1, the state variables (13)–(17) are obtained.

$$v_{L_F}(t) = L_F\frac{di_{L_F}(t)}{dt} = -i_{L_F}(t)\cdot(R_{L_F} + R_D) - V_\gamma + v_{C_{S_2}}(t) - v_{C_F}(t) - i_{C_F}(t)\cdot R_{C_F} \tag{13}$$

$$i_{C_{OSS_1}}(t) = C_{OSS_1}\frac{dv_{C_{OSS_1}}}{dt} = i_{C_{P_1}}(t) + i_{L_{P_1}}(t) - i_{R_{DS_1}}(t) \tag{14}$$

$$i_{C_{OSS_2}}(t) = C_{OSS_2}\frac{dv_{C_{OSS_2}}}{dt} = i_{C_P2}(t) + i_{L_{P_2}}(t) \tag{15}$$

$$i_{C_{S_1}}(t) = C_{S_1}\frac{dv_{C_{S_1}}(t)}{dt} = i_{L_{S_1}}(t) \tag{16}$$

$$i_{C_{S_2}}(t) = C_{S_2}\frac{dv_{C_{S_2}}(t)}{dt} = i_{LS_2}(t) - i_{L_F}(t) \tag{17}$$

where $i_{R_{DS_1}}$ is obtained in the branch of Q_1, (18).

$$i_{R_{DS_1}}(t) = v_{C_{OSS1}}(t)\frac{1}{R_{DS}} \tag{18}$$

For case 2, the state variables (19)–(22) are obtained.

$$i_{C_{OSS_1}}(t) = C_{OSS_1}\frac{dv_{C_{OSS_1}}}{dt} = i_{C_{P_1}}(t) + i_{L_{P_1}}(t) \tag{19}$$

$$i_{C_{OSS_2}}(t) = C_{OSS_2}\frac{dv_{C_{OSS_2}}}{dt} = i_{C_P2}(t) + i_{L_{P_2}}(t) - i_{R_{DS_2}}(t) \tag{20}$$

$$i_{C_{S_1}}(t) = C_{S_1}\frac{dv_{C_{S_1}}(t)}{dt} = i_{LS_1}(t) - i_{L_F}(t) \tag{21}$$

$$i_{C_{S_2}}(t) = C_{S_2} \frac{dv_{C_{S_2}}(t)}{dt} = i_{LS_2}(t) \tag{22}$$

where $i_{R_{DS_2}}$ is obtained in the branch of Q_2, (23).

$$i_{R_{DS_2}}(t) = v_{C_{OSS2}}(t) \frac{1}{R_{DS}} \tag{23}$$

Finally, for case 3, the state variables (24)–(28) are obtained.

$$v_{L_F}(t) = L_F \frac{di_{L_F}(t)}{dt} = -i_{L_F}(t) \cdot \left(R_{L_F} + \frac{R_D}{2} \right) - V_\gamma + v_{C_{S_1}}(t) - v_{C_F}(t) - i_{C_F}(t) \cdot R_{C_F} \tag{24}$$

$$i_{C_{OSS_1}}(t) = C_{OSS_1} \frac{dv_{C_{OSS_1}}}{dt} = i_{C_{P_1}}(t) + i_{L_{P_1}}(t) \tag{25}$$

$$i_{C_{OSS_2}}(t) = C_{OSS_2} \frac{dv_{C_{OSS_2}}}{dt} = i_{C_P2}(t) + i_{L_{P_2}}(t) \tag{26}$$

$$i_{C_{S_1}}(t) = C_{S_1} \frac{dv_{C_{S_1}}(t)}{dt} = i_{LS_1}(t) - i_{L_F}(t) \frac{1}{2} \tag{27}$$

$$i_{C_{S_2}}(t) = C_{S_2} \frac{dv_{C_{S_2}}(t)}{dt} = i_{LS_2}(t) - i_{L_F}(t) \frac{1}{2} \tag{28}$$

Solving the state variables in Equations (1)–(8), (13)–(17), (19)–(22) and (24)–(28) and discretizing them by the Forward Euler method (29), with T_s as the sampling time, (30)–(49) are obtained for the different cases.

$$\frac{dx(t)}{dt} \approx \frac{x(k+1) - x(k)}{T_s} \tag{29}$$

All cases:

$$i_{L_{P_1}}(k+1) = i_{L_{P_1}}(k) \left(1 - T_s \left(\frac{R_{L_P} + R_{Nu}}{L_{P_1}} \right) \right) + i_{L_{P_2}}(k) \frac{T_s \cdot R_{Nu}}{L_{P_1}} + i_{L_M}(k) \frac{T_s \cdot R_{Nu}}{L_{P_1}} - i_{L_{S_1}}(k) \frac{T_s \cdot N \cdot R_{Nu}}{L_{P_1}} + i_{L_{S_2}}(k) \frac{T_s \cdot N \cdot R_{Nu}}{L_{P_1}} - v_{C_{OSS}1}(k) \frac{T_s}{L_{P_1}} + v_{in}(k) \frac{T_s}{L_{P_1}} \tag{30}$$

$$i_{L_{P_2}}(k+1) = i_{L_{P_1}}(t) \frac{T_s \cdot R_{Nu}}{L_{P_2}} + i_{L_{P_2}}(t) \left(1 - T_s \left(\frac{R_{L_P} + R_{Nu}}{L_{P_2}} \right) \right) - i_{L_M}(t) \frac{T_s \cdot R_{Nu}}{L_{P_2}} + i_{L_{S_1}}(t) \frac{T_s \cdot N \cdot R_{Nu}}{L_{P_2}} - i_{L_{S_2}}(t) \frac{T_s \cdot N \cdot R_{Nu}}{L_{P_2}} - v_{C_{OSS}2}(t) \frac{T_s}{L_{P_2}} + v_{in}(t) \frac{T_s}{L_{P_2}} \tag{31}$$

$$i_{L_M}(k+1) = i_{L_{P_1}}(t) \frac{T_s \cdot R_{Nu}}{L_M} - i_{L_{P_2}}(t) \frac{T_s \cdot R_{Nu}}{L_M} + i_{L_M}(k) \left(1 - \frac{T_s \cdot R_{Nu}}{L_M} \right) + i_{L_{S_1}}(t) \frac{T_s \cdot N \cdot R_{Nu}}{L_M} - i_{L_{S_2}}(t) \frac{T_s \cdot N \cdot R_{Nu}}{L_M} \tag{32}$$

$$i_{L_{S_1}}(k+1) = -i_{L_{P_1}}(k) \frac{T_s \cdot N \cdot R_{Nu}}{L_{S_1}} + i_{L_{P_2}}(k) \frac{T_s \cdot N \cdot R_{Nu}}{L_{S_1}} + i_{L_M}(k) \frac{T_s \cdot N \cdot R_{Nu}}{L_{S_1}} + i_{L_{S_1}}(k) \left(1 - T_s \left(\frac{N^2 \cdot R_{Nu} + R_{L_S}}{L_{S_1}} \right) \right) + i_{L_{S_2}}(k) \frac{T_s \cdot N^2 \cdot R_{Nu}}{L_{S_1}} - v_{C_{S_1}}(k) \frac{T_s}{L_{S_1}} \tag{33}$$

$$i_{L_{S_2}}(k+1) = i_{L_{P_1}}(k) \frac{T_s \cdot N \cdot R_{Nu}}{L_{S_2}} - i_{L_{P_2}}(k) \frac{T_s \cdot N \cdot R_{Nu}}{L_{S_2}} - i_{L_M}(k) \frac{T_s \cdot N \cdot R_{Nu}}{L_{S_2}} + i_{L_{S_1}}(k) \frac{T_s \cdot N^2 \cdot R_{Nu}}{L_{S_2}} + i_{L_{S_2}}(k) \left(1 - T_s \left(\frac{N^2 \cdot R_{Nu} + R_{L_S}}{L_{S_2}} \right) \right) - v_{C_{S_2}}(k) \frac{T_s}{L_{S_2}} \tag{34}$$

$$v_{C_P1}(k+1) = v_{C_{P_1}}(k) \left(1 - \frac{T_s}{R_{C_P} \cdot C_{P_1}} \right) - v_{C_{OSS}1}(k) \frac{T_s}{R_{C_P} \cdot C_{P_1}} + v_{in}(k) \frac{T_s}{R_{C_P} \cdot C_{P_1}} \tag{35}$$

$$v_{C_P2}(k+1) = v_{C_{P_2}}(k) \left(1 - \frac{T_s}{R_{C_P} \cdot C_{P_2}} \right) - v_{C_{OSS}2}(k) \frac{T_s}{R_{C_P} \cdot C_{P_2}} + v_{in}(k) \frac{T_s}{R_{C_P} \cdot C_{P_2}} \tag{36}$$

$$v_{C_F}(k+1) = i_{L_F}(k) \left(\frac{T_s}{C_F} \left(\frac{R}{R + R_{C_F}} \right) \right) + v_{C_F}(k) \left(1 - \frac{T_s}{C_F} \left(\frac{1}{(R + R_{C_F})} \right) \right) \tag{37}$$

Case 1 and 2:

$$i_{L_F}(k+1) = i_{L_F}(k)\left(1 - \left(\frac{T_s}{L_F}\left(R_{L_F} + R_D + \frac{R \cdot R_{C_F}}{R + R_{C_F}}\right)\right)\right) + v_{C_S1}(k)\frac{T_s}{L_F} - v_{C_F}(k)\left(\frac{T_s}{L_F}\left(\frac{R}{R + R_{C_F}}\right)\right) - \frac{T_s \cdot V_\gamma}{L_F} \quad (38)$$

Case 3:

$$i_{L_F}(k+1) = i_{L_F}(k)\left(1 - \left(\frac{T_s}{L_F}\left(R_{L_F} + \frac{R_D}{2} + \frac{R \cdot R_{C_F}}{R + R_{C_F}}\right)\right)\right) + v_{C_S1}(k)\frac{T_s}{L_F} - v_{C_F}(k)\left(\frac{T_s}{L_F}\left(\frac{R}{R + R_{C_F}}\right)\right) - \frac{T_s \cdot V_\gamma}{L_F} \quad (39)$$

Case 1:

$$v_{C_{OSS_1}}(k+1) = i_{L_{P_1}}(k)\frac{T_s}{C_{OSS_1}} - v_{C_{P_1}}(k)\frac{T_s}{R_{C_P} \cdot C_{OSS_1}} + v_{C_{OSS}1}(k)\left(1 - T_s\left(\frac{1}{R_{C_P} \cdot C_{OSS_1}} + \frac{1}{R_{DS} \cdot C_{OSS_1}}\right)\right) + \\ v_{in}(k)\frac{T_s}{R_{C_P} \cdot C_{OSS_1}} \quad (40)$$

Cases 2 and 3:

$$v_{C_{OSS_1}}(k+1) = i_{L_{P_1}}(k)\frac{T_s}{C_{OSS_1}} - v_{C_{P_1}}(k)\frac{T_s}{R_{C_P} \cdot C_{OSS_1}} + v_{C_{OSS}1}(k)\left(1 - \left(\frac{T_s}{R_{C_P} \cdot C_{OSS_1}}\right)\right) + v_{in}(k)\frac{T_s}{R_{C_P} \cdot C_{OSS_1}} \quad (41)$$

Cases 1 and 3:

$$v_{C_{OSS2}}(k+1) = i_{L_{P_2}}(k)\frac{T_s}{C_{OSS_2}} - v_{C_{P_2}}(k)\frac{T_s}{R_{C_P} \cdot C_{OSS_2}} + v_{C_{OSS}2}(k)\left(1 - \frac{T_s}{R_{C_P} \cdot C_{OSS_2}}\right) + v_{in}(k)\frac{T_s}{R_{C_P} \cdot C_{OSS_2}} \quad (42)$$

Case 2:

$$v_{C_{OSS2}}(k+1) = i_{L_{P_2}}(k)\frac{T_s}{C_{OSS_2}} - v_{C_{P_2}}(k)\frac{T_s}{R_{C_P} \cdot C_{OSS_2}} + v_{C_{OSS}2}(k)\left(1 - T_s\left(\frac{1}{R_{C_P} \cdot C_{OSS_2}} + \frac{1}{R_{DS} \cdot C_{OSS_2}}\right)\right) + \\ v_{in}(k)\frac{T_s}{R_{C_P} \cdot C_{OSS_2}} \quad (43)$$

Case 1:

$$v_{C_{S1}}(k+1) = i_{L_{S_1}}(k)\frac{T_s}{C_{S_1}} + v_{C_{S1}}(k) \quad (44)$$

Case 2:

$$v_{C_{S1}}(k+1) = i_{L_{S_1}}(k)\frac{T_s}{C_{S_1}} - i_{L_F}(k)\frac{T_s}{C_{S_1}} + v_{C_{S1}}(k) \quad (45)$$

Case 3:

$$v_{C_{S1}}(k+1) = i_{L_{S_1}}(k)\frac{T_s}{C_{S_1}} - i_{L_F}(k)\frac{T_s}{2C_{S_1}} + v_{C_{S1}}(k) \quad (46)$$

Case 1:

$$v_{C_{S2}}(k+1) = i_{L_{S_2}}(k)\frac{T_s}{C_{S_2}} - i_{L_F}(k)\frac{T_s}{C_{S_2}} + v_{C_{S2}}(k) \quad (47)$$

Case 2:

$$v_{C_{S2}}(k+1) = i_{L_{S_2}}(k)\frac{T_s}{C_{S_2}} + v_{C_{S2}}(k) \quad (48)$$

Case 3:

$$v_{C_{S2}}(k+1) = i_{L_{S_2}}(k)\frac{T_s}{C_{S_2}} - i_{L_F}(k)\frac{T_s}{2C_{S_2}} + v_{C_{S2}}(k) \quad (49)$$

2.4. Discrete State-Space Model

By means of (30)–(49), the three SIMO state models corresponding to the three cases can be obtained. Then, considering the well-known expression of the equation of state, $x(k+1) = Ax(k) + Bu(k) + E$, and the output, $y(k) = Cx(k) + Du(k)$, the state vector, ordering by currents and voltages, will be (50):

$$x = [i_{L_{P_1}}, i_{L_{P_2}}, i_{L_M}, i_{L_{S_1}}, i_{L_{S_2}}, i_{L_F}, v_{C_{P_1}}, v_{C_{P_2}}, v_{C_{OSS1}}, v_{C_{OSS2}}, v_{C_{S_1}}, v_{C_{S_2}}, v_{C_F}]^T \quad (50)$$

where, for ease of editing, the dependence on k is omitted. Regarding input and output vectors, see Figure 3, $u(k) = v_{in}(k)$ and $y(k) = [v_R(k) \; i_R(k)]^T$. This output vector facilitates the use of the model for the usual control, i.e., in current or voltage (both variables can be easily measured). From here, for the three cases, the Equations (51)–(53) are obtained. Note that the three state matrices are configured in the form of rows (i = 1 to 13) as follows: $A_{\lambda_i} = \left[A_{\lambda_1} \; A_{\lambda_2} \ldots A_{\lambda_{13}} \right]^T$, where, depending on the case, $\lambda = 1, 2, 3$.

Case 1 (commas separate columns):

$$A_{1_1} = \left[1 - T_s \left(\frac{R_{L_P} + R_{Nu}}{L_{P_1}} \right), \frac{T_s \cdot R_{Nu}}{L_{P_1}}, \frac{T_s \cdot R_{Nu}}{L_{P_1}}, -\frac{T_s \cdot N \cdot R_{Nu}}{L_{P_1}}, \frac{T_s \cdot N \cdot R_{Nu}}{L_{P_1}}, 0,0,0, -\frac{T_s}{L_{P_1}}, 0,0,0,0 \right]$$

$$A_{1_2} = \left[\frac{T_s \cdot R_{Nu}}{L_{P_2}}, 1 - T_s \left(\frac{R_{L_P} + R_{Nu}}{L_{P_2}} \right), -\frac{T_s \cdot R_{Nu}}{L_{P_2}}, \frac{T_s \cdot N \cdot R_{Nu}}{L_{P_2}}, -\frac{T_s \cdot N \cdot R_{Nu}}{L_{P_2}}, 0,0,0,0, -\frac{T}{L_{P_2}}, 0,0,0 \right]$$

$$A_{1_3} = \left[\frac{T_s \cdot R_{Nu}}{L_M}, -\frac{T_s \cdot R_{Nu}}{L_M}, 1 - \frac{T_s \cdot R_{Nu}}{L_M}, \frac{T_s \cdot N \cdot R_{Nu}}{L_M}, -\frac{T_s \cdot N \cdot R_{Nu}}{L_M}, 0,0,0,0,0,0,0,0 \right]$$

$$A_{1_4} = \left[-\frac{T_s \cdot N \cdot R_{Nu}}{L_{S_1}}, \frac{T_s \cdot N \cdot R_{Nu}}{L_{S_1}}, \frac{T_s \cdot N \cdot R_{Nu}}{L_{S_1}}, 1 - T_s \left(\frac{N^2 \cdot R_{Nu} + R_{L_S}}{L_{S_1}} \right), \frac{T_s \cdot N^2 \cdot R_{Nu}}{L_{S_1}}, 0,0,0,0,0, -\frac{T_s}{L_{S_1}}, 0,0 \right]$$

$$A_{1_5} = \left[\frac{T_s \cdot N \cdot R_{Nu}}{L_{S_2}}, -\frac{T_s \cdot N \cdot R_{Nu}}{L_{S_2}}, -\frac{T_s \cdot N \cdot R_{Nu}}{L_{S_2}}, \frac{T_s \cdot N^2 \cdot R_{Nu}}{L_{S_2}}, 1 - T_s \left(\frac{N^2 \cdot R_{Nu} + R_{L_S}}{L_{S_2}} \right), 0,0,0,0,0,0, -\frac{T_s}{L_{S_2}}, 0 \right]$$

$$A_{1_6} = \left[0,0,0,0,0, 1 - \left(\frac{T_s}{L_F} \left(R_{L_F} + R_D + \frac{R \cdot R_{C_F}}{R + R_{C_F}} \right) \right), 0,0,0,0,0, \frac{T_s}{L_F}, -\frac{T_s}{L_F} \left(\frac{R}{R + R_{C_F}} \right) \right]$$

$$A_{1_7} = \left[0,0,0,0,0,0, 1 - \frac{T_s}{R_{C_P} \cdot C_{P_1}}, 0, -\frac{T_s}{R_{C_P} \cdot C_{P_1}}, 0,0,0,0 \right]$$

$$A_{1_8} = \left[0,0,0,0,0,0,0, 1 - \frac{T_s}{R_{C_P} \cdot C_{P_2}}, 0, -\frac{T_s}{R_{C_P} \cdot C_{P_2}}, 0,0,0 \right]$$

$$A_{1_9} = \left[\frac{T_s}{C_{OSS_1}}, 0,0,0,0,0, -\frac{T_s}{R_{C_P} \cdot C_{OSS_1}}, 0, 1 - T_s \left(\frac{1}{R_{C_P} \cdot C_{OSS_1}} + \frac{1}{R_{DS} \cdot C_{OSS_1}} \right), 0,0,0,0 \right]$$

$$A_{1_{10}} = \left[0, \frac{T_s}{C_{OSS_2}}, 0,0,0,0,0, -\frac{T_s}{R_{C_P} \cdot C_{OSS_2}}, 0, 1 - T_s \left(\frac{1}{R_{C_P} \cdot C_{OSS_2}} \right), 0,0,0 \right]$$

$$A_{1_{11}} = \left[0,0,0, \frac{T_s}{C_{S_1}}, 0,0,0,0,0,0, 1,0,0 \right]$$

$$A_{1_{12}} = \left[0,0,0,0, \frac{T_s}{C_{S_2}}, -\frac{T_s}{C_{S_2}}, 0,0,0,0,0, 1,0 \right]$$

$$A_{1_{13}} = \left[0,0,0,0,0, \frac{T_s}{C_F} \left(\frac{R}{R + R_{C_F}} \right), 0,0,0,0,0,0, 1 - \frac{T_s}{C_F} \left(\frac{1}{(R + R_{C_F})} \right) \right]$$

(51)

Case 2 = case 1 for $A_{2_\alpha} = A_{1_\alpha}$, $\alpha = 1, \ldots 8$ and 13 :

$$A_{2_9} = \left[\frac{T_s}{C_{OSS_1}}, 0,0,0,0,0, -\frac{T_s}{R_{C_P} \cdot C_{OSS_1}}, 0, 1 - T_s \left(\frac{1}{R_{C_P} \cdot C_{OSS_1}} \right), 0,0,0,0 \right]$$

$$A_{2_{10}} = \left[0, \frac{T_s}{C_{OSS_2}}, 0,0,0,0,0, -\frac{T_s}{R_{C_P} \cdot C_{OSS_2}}, 0, 1 - T_s \left(\frac{1}{R_{C_P} \cdot C_{OSS_2}} + \frac{1}{R_{DS} \cdot C_{OSS_2}} \right), 0,0,0 \right]$$

$$A_{2_{11}} = \left[0,0,0, \frac{T_s}{C_{S_1}}, 0, -\frac{T_s}{C_{S_1}}, 0,0,0,0, 1,0,0 \right]$$

$$A_{2_{12}} = \left[0,0,0,0, \frac{T_s}{C_{S_2}}, 0,0,0,0,0,0, 1,0 \right]$$

(52)

Case 3 = case 1 for $A_{3_\alpha} = A_{1_\alpha}$, $\alpha = 1, \ldots 5; \; 7, \ldots 10$ and 13.

$$A_{3_6} = \left[0,0,0,0,0, 1 - \left(\frac{T_s}{L_F} \left(R_{L_F} + \frac{R_D}{2} + \frac{R \cdot R_{C_F}}{R + R_{C_F}} \right) \right), 0,0,0,0, \frac{T_s}{L_F}, 0, -\frac{T_s}{L_F} \left(\frac{R}{R + R_{C_F}} \right) \right]$$

$$A_{3_{11}} = \left[0,0,0, \frac{T_s}{C_{S_1}}, 0, -\frac{T_s}{2C_{S_1}}, 0,0,0,0, 1,0,0 \right]$$

$$A_{3_{12}} = \left[0,0,0,0, \frac{T_s}{C_{S_2}}, -\frac{T_s}{2C_{S_2}}, 0,0,0,0,0, 1,0 \right]$$

(53)

For all cases, matrices B and E are shown in (54) and (55), respectively.

$$B = \left[\frac{T_s}{L_{P_1}}, \frac{T_s}{L_{P_2}}, 0,0,0,0, \frac{T_s}{R_{C_P} \cdot C_{P_1}}, \frac{T_s}{R_{C_P} \cdot C_{P_2}}, \frac{T_s}{R_{C_P} \cdot C_{OSS_1}}, \frac{T_s}{R_{C_P} \cdot C_{OSS_2}}, 0,0,0 \right]^T$$

(54)

$$E = \left[0,0,0,0,0, -\frac{T_s \cdot V_\gamma}{L_F}, 0,0,0,0,0,0,0 \right]^T$$

(55)

Finally, the outputs of the system (see Figure 3) are given by (56) and (57).

$$v_R(k) = i_{CF}(k) \cdot R_{C_F} + v_{C_F}(k) = i_{L_F}(k) \left(\frac{R \cdot R_{C_F}}{R + R_{C_F}} \right) + v_{C_F}(k) \left(\frac{R}{R + R_{C_F}} \right)$$

(56)

$$i_R(k) = \frac{v_R(k)}{R} = i_{L_F}(k)\left(\frac{R_{C_F}}{R + R_{C_F}}\right) + v_{C_F}(k)\left(\frac{1}{R + R_{C_F}}\right) \tag{57}$$

Hence, the matrices of the model output equation are given by (58), where the semicolon separates the rows.

$$C = \left[0,0,0,0,0, \frac{R \cdot R_{C_F}}{R + R_{C_F}}, 0,0,0,0,0,0, \frac{R}{R + R_{C_F}}; 0,0,0,0,0, \frac{R_{C_F}}{R + R_{C_F}}, 0,0,0,0,0,0, \frac{1}{R + R_{C_F}}\right]$$
$$D = [0,0]^T \tag{58}$$

2.5. Average Discrete State-Space Model

Since the duty cycle of the converter is $d = t_{on}/T$, where t_{on} is the activation time of any of the electronic switches of the converter (Q_1 or Q_2 ON), and T is the time of a complete converter cycle (in this, the converter goes through the three cases or modes of operation) and, theoretically, $0 \leq d \leq 1$, the average model in T is as shown in (59).

$$\begin{aligned} x(k+1) &= \overline{A} \cdot x(k) + \overline{B} \cdot u(k) + \overline{E} \\ y(k) &= \overline{C} \cdot x(k) + \overline{D} \cdot u(k) \end{aligned} \tag{59}$$

where each of the three cases contribute as follows:

$$\begin{aligned} \overline{A} &= A_1 \cdot d + A_2 \cdot d + A_3(1 - 2d) \\ \overline{B} &= B \cdot d + B \cdot d + B(1 - 2d) \\ \overline{E} &= E \cdot d + E \cdot d + E(1 - 2d) \\ \overline{C} &= C \\ \overline{D} &= D \end{aligned} \tag{60}$$

where $1 - 2d$ is the corresponding cycle for Q_1 and Q_2 OFF.

Entering (51)–(53) and (55) in (60), and during operation, with $\overline{A} = \begin{bmatrix} \overline{A_1} \ \overline{A_2} \dots \overline{A_{13}} \end{bmatrix}^T$, (61) is obtained.

$$\begin{aligned} \overline{A_1} &= A_{1_1}; \ \overline{A_2} = A_{1_2}; \overline{A_3} = A_{1_3}; \ \overline{A_4} = A_{1_4}; \ \overline{A_5} = A_{1_5}; \\ \overline{A_6} &= \left[0,0,0,0,0, 1 - \left(\frac{T_s}{L_F}\left(R_{L_F} + R_D\left(\frac{1}{2} + d\right) + \frac{R \cdot R_{C_F}}{R + R_{C_F}}\right)\right), 0,0,0,0, \frac{T_s}{L_F}(1 - 2d), \frac{T_s}{L_F}2d, -\frac{T_s}{L_F}\left(\frac{R}{R + R_{C_F}}\right)\right] \\ \overline{A_7} &= A_{1_7}; \ \overline{A_8} = A_{1_8}; \\ \overline{A_9} &= \left[\frac{T_s}{C_{OSS_1}}, 0,0,0,0,0, -\frac{T_s}{R_{C_P} \cdot C_{OSS_1}}, 0, 1 - T_s\left(\frac{1}{R_{C_P} \cdot C_{OSS_1}} + \frac{1 - d}{R_{DS} \cdot C_{OSS_1}}\right), 0,0,0,0\right] \\ \overline{A_{10}} &= \left[0, \frac{T_s}{C_{OSS_2}}, 0,0,0,0,0, -\frac{T_s}{R_{C_P} \cdot C_{OSS_2}}, 0, 1 - T_s\left(\frac{1}{R_{C_P} \cdot C_{OSS_2}} + \frac{d}{R_{DS} \cdot C_{OSS_2}}\right), 0,0,0\right] \\ \overline{A_{11}} &= A_{3_{11}}; \ \overline{A_{12}} = A_{3_{12}}; \ \overline{A_{13}} = A_{1_{13}} \\ \overline{E} &= E \end{aligned} \tag{61}$$

2.6. Discrete Small-Signal Model

The discrete small-signal model of the converter is obtained by assuming a perturbation with respect to an operating point in the state variables, output variables, input variables and duty cycle. This allows for the variables to be written as (62), i.e., as the sum of their value at the operating point (X, Y, U, D), in addition to a perturbation that generates ($\hat{x}, \hat{y}, \hat{u}, \hat{d}$).

$$x = X + \hat{x}; \ y = Y + \hat{y}; \ u = U + \hat{u}; \ d = D + \hat{d} \tag{62}$$

where x is given by (50) and the rest by (63).

$$\begin{aligned} X &= \left[I_{L_{P_1}}, I_{L_{P_2}}, I_{L_M}, I_{L_{S_1}}, I_{L_{S_2}}, I_{L_F}, V_{C_{P_1}}, V_{C_{P_2}}, V_{C_{OSS_1}}, V_{C_{OSS_2}}, V_{C_{S_1}}, V_{C_{S_2}}, V_{C_F}\right]^T \\ \hat{x} &= \left[\hat{i}_{L_{P_1}}, \hat{i}_{L_{P_2}}, \hat{i}_{L_M}, \hat{i}_{L_{S_1}}, \hat{i}_{L_{S_2}}, \hat{i}_{L_F}, \hat{v}_{C_{P_1}}, \hat{v}_{C_{P_2}}, \hat{v}_{C_{OSS_1}}, \hat{v}_{C_{OSS_2}}, \hat{v}_{C_{S_1}}, \hat{v}_{C_{S_2}}, \hat{v}_{C_F}\right]^T \\ y &= [v_R \ i_R]^T; \quad Y = [V_R \ I_R]^T; \quad \hat{y} = [\hat{v}_R \ \hat{i}_R] \\ u &= v_{in}; \quad U = V_{in}; \quad \hat{u} = \hat{v}_{in} \end{aligned} \tag{63}$$

Now, from (59) and (60), the following equation obtained (64).

$$x(k+1) = X + \hat{x}(k+1) = \left[A_1 \cdot \left(D + \hat{d} \right) + A_2 \cdot \left(D + \hat{d} \right) + A_3 \cdot \left(1 - 2 \left(D + \hat{d} \right) \right) \right] \cdot [X + \hat{x}(k)] + [B \cdot \left(D + \hat{d} \right) +$$
$$B \cdot \left(D + \hat{d} \right) + B \cdot \left(1 - 2 \left(D + \hat{d} \right) \right)] \cdot [U + \hat{u}(k)] + \left[E \cdot \left(D + \hat{d} \right) + E \cdot \left(D + \hat{d} \right) + E \cdot \left(1 - 2 \left(D + \hat{d} \right) \right) \right] \quad (64)$$
$$Y + \hat{y}(k) = C[X + \hat{x}(k)] + D[U + \hat{u}(k)]$$

From term to term, (64) can be written as (65), i.e., a constant term that depends on the system at its operating point (OP_x/OP_y), plus a linear term that depends on the perturbed system (L_x/L_y), plus a nonlinear term that depends on the perturbed system (NL_x).

$$X + \hat{x}(k+1) = OP_x(X, U) + L_x \left(\hat{x}(k), \hat{u}(k), \hat{d} \right) + NL_x \left(\left(\hat{x}(k), \hat{d} \right) \right)$$
$$Y + \hat{y}(k) = OP_y(X, U) + L_y(\hat{x}(k), \hat{u}(k)) \quad (65)$$

where OPx/y, Lx/y and NL are given, respectively, by (66).

$$OP_x = [A_1 \cdot D \cdot X + A_2 \cdot D \cdot X + A_3 \cdot (1 - 2D)X + [B \cdot U] + E]$$
$$L_x = [A_1 \cdot D + A_2 \cdot D + A_3 \cdot (1 - 2D)]\hat{x}(k) + B \cdot \hat{u}(k) + [A_1 \cdot X + A_2 \cdot X - 2A_3 \cdot X] \cdot \hat{d}$$
$$NL_x = [A_1 + A_2 - 2A_3]\hat{d} \cdot \hat{x}(k)$$
$$\text{And for the output,} \quad (66)$$
$$OP_y = C \cdot X + D \cdot U$$
$$L_y = C \cdot \hat{x}(k) + D \cdot \hat{u}(k)$$

Since the model sought is dynamic, the constant terms (equilibrium state) are of no interest, because, without any loss of generality, they can be taken to point 0 of the state-space. On the other hand, the nonlinear term consists of the product of two very small magnitudes, so it can be ignored without losing practical accuracy. As a result, (65) can be written as (67), which represents the small-signal linear model of the converter in Figure 2.

$$\hat{x}(k+1) = \underbrace{[A_1 \cdot D + A_2 \cdot D + A_3 \cdot (1 - 2D)]}_{\hat{A}}\hat{x}(k) + B \cdot \hat{u}(k)\underbrace{[(A_1 + A_2 - 2A_3)X]}_{\hat{E}}\hat{d}$$
$$\hat{y}(k) = C \cdot \hat{x}(k) + D \cdot \hat{u}(k) \quad (67)$$

Regarding the perturbations, both $\hat{u}$ and $\hat{d}$ can be considered inputs, so an extended input vector ($\hat{u}_e$) including both can be considered. Thus, (67) can be written as in (68).

$$\hat{x}(k+1) = \hat{A} \cdot \hat{x}(k) + \hat{B} \cdot \hat{u}_e(k)$$
$$\hat{y}(k) = C \cdot \hat{x}(k) + D \cdot \hat{u}(k) \quad (68)$$

where

$$\hat{B} = \left[B, \hat{E} \right]; \hat{u}_e(k) = \left[\hat{v}_{in}; \hat{d} \right]$$

3. Results

To evaluate and validate the performance of the developed dynamic model of the push–pull converter, two experimental tests were carried out on a real 2 kW converter. This converter was specifically developed by the authors for this application to learn all its parameters. Two tests were performed to evaluate the steady-state behavior of the converter, considering variations in the converter input voltage (test 1) and in its duty cycle (test 2). The objective of both tests was to evaluate the performance of the developed model with respect to variations in each variable in isolation. Finally, a dynamic performance test (test 3) was developed. These tests will be described in more detail below.

The validation of the model consisted of comparing the results of the open-loop simulations of the developed model (DM) with the experimental results obtained (Exp) in the real converter. On the other hand, to demonstrate the performance of the developed model with respect to existing solutions in the scientific literature, these results were

also compared with those obtained using the ideal model (IM) developed in [17] and the reference model (RM), represented by the most complete T3M found in the literature [23].

For the instrumentation systems required for the experimental tests, the following were used: a Regatron® programmable power (Regatron, Rorschach, Switzerland.) supply (TC.GSS series) to generate the input voltage to the converter and a LeCroy® WaveSurfer 454 oscilloscope (Lecroy, New York, USA) with a professional current and differential voltage probes to measure the electrical variables in the converter. The converter load was implemented using a bank of eight power resistors of 10 Ω, with each connected in series. Finally, the switching frequency of the converter's PWM signal was set at 25 kHz, which is typical for converters in this power range. The experimental setup is shown in Figure 4.
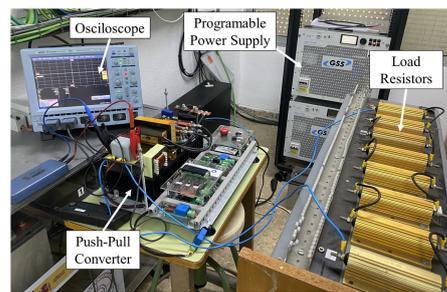

Figure 4. Laboratory experimental set-up.

On the other hand, all simulations were performed in the Matlab® environment. The sampling time was set at 5 μs.

Finally, the converter parameters were obtained from the component datasheets, as well as from direct measurements in the actual circuit. In the specific case of the HF transformer, the capacitances and leakage inductances were calculated from empirical expressions based on the transformer construction and sizing according to [30,31], respectively, while the core parameters were calculated by performing an open-circuit test. Hardware details are shown in Table 2.

Table 2. Push–pull converter parameters.

Element	Model and Characteristics	Parameter
Capacitor filter	MKP1848680704Y5, Vishay® (Vishay, Hangzhou, China) Power voltage: 700 VDC	C_F : 80 μF R_{C_F} : 3 mΩ
Inductance filter	Custom Ferrite material: N27	L_F : 2.1 mH R_{L_F} : 30 mΩ
HF transformer	Custom, Saber S.L.® (Saber, Barcelona, Spain) Ferrite material: N27 Core: E100/60/28 Winding turns ratio: 1:12	N_P : 4 N_S : 48 L_P : 0.4 μH L_S : 70 μH R_{L_P} : 8.5 mΩ R_{L_S} : 470 mΩ C_P : 40 pF C_S : 40 pF L_M : 500 μH R_{Nu} : 200 kΩ
Load resistor	HS300 10R F, Arcol® (Arcol, Warrenville, Illinois, USA) Configuration: 8S1P Power rating: 300 W	R : 80 Ω
Mosfet	IXFN132N50P3, IXYS® (YXIS, Milpitas, California, USA) Configuration: 2S1P Maximum voltage: 500 V Maximum current: 112 A	R_{DS} : 40 mΩ C_{oss} : 3.5 nF
Rectifier diode	VS-20ETF12PbF, Vishay® (Vishay, Hangzhou, China) Configuration: 2S1P Maximum voltage: 1200 V Maximum current: 20 A	R_D : 21 mΩ V_γ : 1.1 V

The tests carried out for the comparison and validation of the developed model are detailed below.

Test 1. Steady-state response to changes in input voltage with a constant duty cycle.

The purpose of this test is to validate the steady-state response of the DM with respect to variations in the input voltage of the converter. To this end, the test consisted of applying a variable input voltage profile to the real converter (Exp) and that of the different models (DM, IM, and RM). This profile is characterized by voltage steps in the 0–50 VDC range. To isolate the effect of duty cycle variations on the converter dynamics, its value was kept constant at 30%. The results of test 1 are shown in Figure 5.
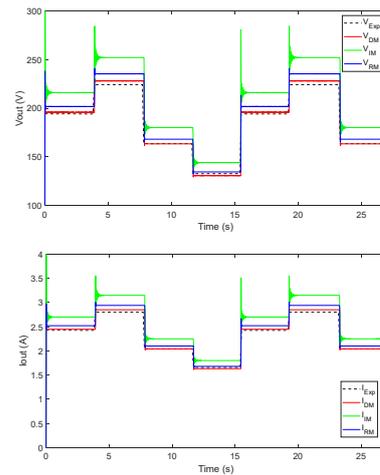
Figure 5. Test 1. Output voltage (**top** plot) and current (**bottom** plot) response for the real converter (Exp), the developed model (DM), the ideal model (IM) and the reference model (RM) for an input voltage variation profile in the 0–50 VDC range at a constant duty cycle of 30%.

Test 2. Steady state response to changes in duty cycle with constant input voltage.

In this case, the purpose of this test is to validate the steady-state response of the DM with respect to variations in the converter duty cycle. To this end, the test consisted of applying a variable duty cycle profile to the real converter (Exp) and that of the different models (DM, IM, and RM). This profile is characterized by duty cycle steps ranging from 20% to 35%. To isolate the effect of input voltage variations on the converter dynamics, its value was kept constant at 30 VDC. The results of test 2 are shown in Figure 6.
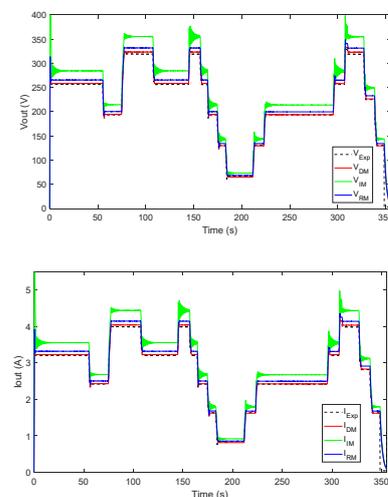

Figure 6. Test 2. Output voltage (**top** plot) and current (**bottom** plot) response for the actual converter (Exp), the developed model (DM), the ideal model (IM) and the reference model (RM) for a duty cycle variation profile in the 20–35% range at a constant input voltage of 30 VDC.

Test 3. Dynamic analysis.

Finally, the objective of this test was to validate the dynamic behavior of the DM. To this end, the test consisted of analyzing the transient response of the converter output variables for an increase in the duty cycle of the real converter (Exp) and that of the different models (DM, IM, and RM). Specifically, the test corresponds to the duty cycle change in test 2 at t = 15.40 s. The results of test 3 are shown in Figure 7.
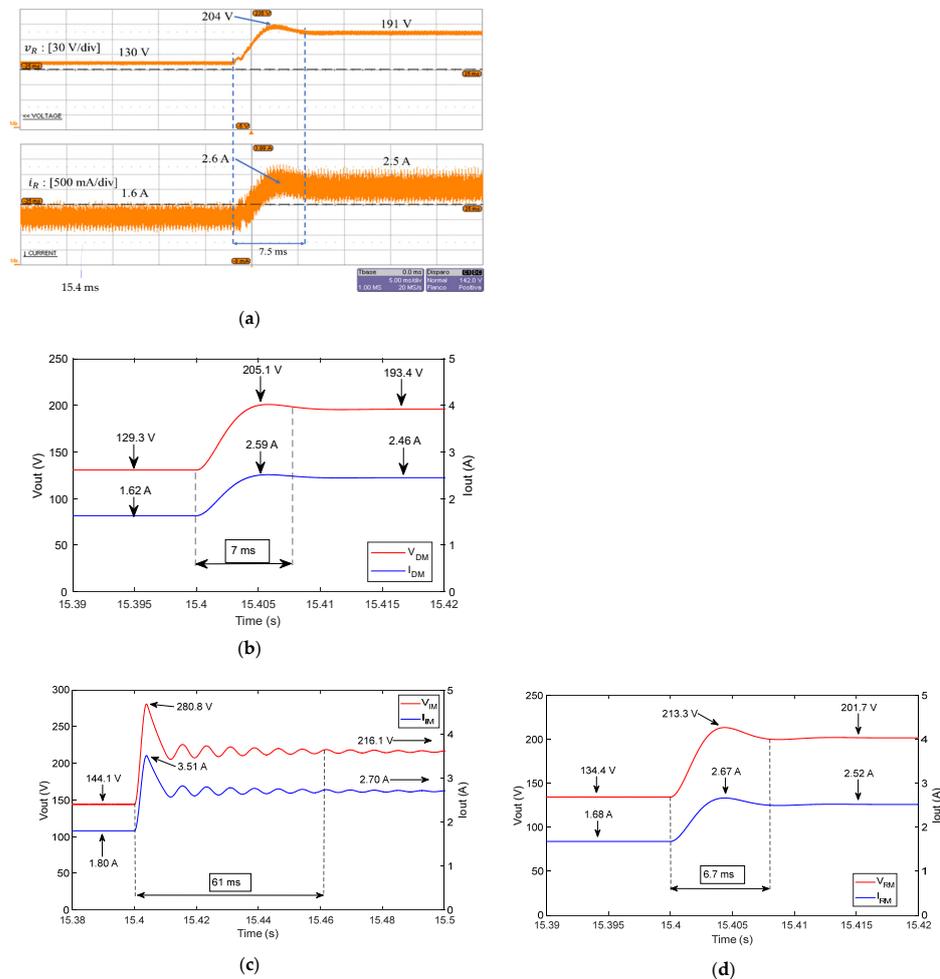

Figure 7. Test 3. Dynamic analysis of the converter output voltage and current for a duty cycle step. (**a**) Real converter, (**b**) developed model (DM), (**c**) ideal model (IM) and (**d**) reference model (RM).

4. Discussion

In this section, the results obtained for the three previously defined tests will be analyzed and discussed. Following the order of the tests, the results of the steady-state behavior evaluation tests, tests 1 and 2, will be analyzed and discussed first.

First, as a naked-eye analysis, the DM shows excellent performance, with the best results of all the models in all the performed tests. This is clearly reflected by the evolution of the converter output voltage and current variables (Figures 5–7).

In more detail, compared to IM and RM, Figures 5 and 6 show that DM performs considerably better in both tests for both output variables. In fact, the responses of DM and the real converter (Exp) practically overlap. With respect to the results obtained for IM and RM, it is observed that, in all cases, the output voltages and, therefore, the output currents, are higher than those of the DM and the real converter. These differences, or steady-state errors, are explained by the fact that the IM and RM models do not consider all voltage drops inside the converter due to their non-idealities. Namely, and among others,

internal losses are obtained in the parasitic resistors of electronic switches and other passive components, as well as in the forward voltage drop of across the rectifier diodes.

According to the obtained results, and as would be expected, the magnitude of the steady-state error is closely related to the number of simplifications made in the definition of the model. The smaller the number of non-idealities in the model (the greater the simplifications), the greater the steady-state error. This behavior is noticeable in Figures 5 and 6 and is also evident from the statistical analysis of model error for both output variables in Table 3.

Table 3. Developed and reference model comparison. Analysis of errors.

N° Test	Variable	Developed Model (DM)			Ideal Model (IM)			Reference Model (RM)		
		RMSE	MAE	MAPE (%)	RMSE	MAE	MAPE (%)	RMSE	MAE	MAPE (%)
1	v_R	8.625	1.468	1.722	30.20	24.87	11.456	11.89	7.939	3.982
	i_R	0.119	0.055	2.680	0.407	0.347	13.291	0.174	0.136	5.636
2	v_R	2.517	1.344	1.034	21.55	20.76	10.973	7.770	7.020	2.507
	i_R	0.064	0.059	2.507	0.310	0.302	13.138	0.136	0.130	5.618

For the correct interpretation of the statistical analysis, it is necessary to consider that both the mean absolute error (MAE) and the root mean square error (RMSE) provide information on absolute, not relative, errors. This makes the behavior of all models appear better for the output current variable than for the output voltage. However, this is due to the different magnitudes, and therefore scales, in Figures 5 and 6. Consequently, to ensure a better appreciation of the magnitude of the error and comparison between models, the mean absolute percentage error ($MAPE$) is included (69). The application of this statistic shows that the behavior is the opposite, which is logical: the lower the internal voltage drops for the same input voltage, the higher the current available at the output.

$$MAPE = \frac{100\%}{n} \sum_{n=1}^{n} \left| \frac{Real - Model}{Real} \right| \tag{69}$$

In view of the above, and as expected, the completeness of the DM definition guarantees a close approximation of the actual converter behavior. In the opposite direction, the error rate of RM and IM is closely linked to the number of simplifications adopted, with IM clearly showing a higher deviation.

The results of the dynamic response test, test 3, will now be analyzed and discussed.

Based on the results obtained for test 3, the dynamic behavior of the output variables for an increasing duty cycle jump (at t = 15.40 s, Figure 7) is characterized by an under-damped response in the real converter, as shown in Figure 7a. This dynamic response is mainly imposed by the second-order low-pass filter at the converter output, while the overshoot, settling time and steady-state value are defined by the effect of the converter's non-idealities. This behavior is also observed in all models, although it should be noted that, in the case of the IM, there is a noticeable overshoot, followed by a long-lasting oscillatory response (Figure 7c).

As in tests 1 and 2, the dynamic behavior of the converter is strongly influenced by the effect of the non-idealities considered during the modelling phase. In this case, parasitic resistances, capacitances, and inductances will have a significant effect on the dynamic response of the output voltage and current. Again, the greater the number of adopted simplifications, the greater the divergence between the experimental response of the converter and that simulated by the models. This is clearly seen in the comparison between the dynamic responses of the experimental converter and the models, as shown in Figure 7. In particular, the overvoltage and overcurrent in the real case reached 6.81% and 4.00% respectively, compared to the 6.05% and 5.28% achieved by DM (Figure 7b) and 5.75% and 5.95% achieved by RM (Figure 7d), which were both very similar. However,

both models show more pronounced differences in the final value at steady-state. Thus, the values provided by the DM (194.4 V and 2.43 A) are much closer to those of the real converter (191 V and 2.5 A) than the MR (201.7 V and 2.52 A). Finally, for the settling time (99%), the DM (7 ms) is closer to the real case (7.5 ms) than the RM (6.7 ms).

Regarding the dynamic behavior of the IM with respect to the real converter and the other two models (DM and RM), Figure 7c shows that it does not support a reasonable comparison, as its results are far from what could be considered minimum acceptable behavior. That is, the IM is not valid for the dynamic analysis of push–pull converters.

From the results, it is concluded that the DM allows for the dynamic and steady-state behavior of the push-pull converter to be modeled with high accuracy and are shown to have a better performance than the reference models studied in the scientific literature. Moreover, the accuracy of the DM is likely to be even higher than that shown in these graphs and tables. The reason for this is obvious and practical. The real converter and the experimental setup have additional resistances, inductances, and parasitic capacitances (not accounted for in the DM) associated with the wiring, connectors, and printed circuit board. The only notable discrepancy between the response of the real converter and the DM is liekly that the DM is not able to simulate the output current and voltage ripple due to the absence of switching frequency in the model.

Finally, it is questionable whether the addition of non-idealities and losses to the model should lead to more than the three analyzed being considered. Of course, the magnetization and demagnetization of the primary and secondary windings of the transformer could generate transient microstates of microseconds or less. The number of microstates that could be generated is very difficult to evaluate, since the casuistry would be diverse. However, based on the obtained results, this has no practical effect on the quality of the model, so it has not been considered.

Finally, although simulation time is not a determining criterion in this work, the models can be compared according to the computational cost to evaluate their performance as simulation and control tools.

Thus, for test 1, simulation times of 3.39 s, 3.75 s and 5.16 s were obtained for IM, RM and PM, respectively. For test 2, simulation times of 14.65 s, 15.24 s and 18.66 s were obtained for MI, RM and PM, respectively.

From the results, the inclusion of non-idealities increases the order and complexity of the model and, therefore, the computational cost. Considering the simulation times obtained in a laptop with standard characteristics, there is no criticality regarding the use of PM as a simulation tool.

5. Conclusions

This paper presents a general, complete, and very accurate state-space dynamic model of a push–pull converter. In contrast to the works reviewed in the scientific literature, which present simplified models designed around certain operating conditions, the proposed model considers all the practical non-idealities present in any push–pull converter due to the transformer, the switching devices (electronic switches and diodes) and the other passive elements.

The state-space formulation that was developed confers modularity, versatility, and computability to the model and, despite its high order, it is essentially simple, orderly, intuitive and, above all, very practical. In addition, the model is adaptive, so it can follow the intrinsically nonlinear behavior of the converter, depending on the operating conditions (voltage, current and temperature) for each sampling time. This means that there can be a different model at every sampling time, which is possible in practice because its formulation does not require a very high computational burden. Therefore, the developed model opens the door to the design of model-based adaptive controllers for the more efficient real-time control of power systems. In addition, the developed model allows for the construction of accurate push–pull converter simulators that, being adaptive and capable of running in real-time, allow, with the appropriate sensing, for the implementation of digital twins.

The performance of the developed model was evaluated and validated against a real 2 kW push–pull converter. Steady-state and dynamic response tests were carried out for variations in both the converter input signal and duty cycle, respectively. The performance of the developed model was also compared with reference models that are widely used in the scientific literature. The developed model had an excellent performance, with mean absolute percentage errors below 2.7% in all cases, considerably lower than the error of the reference models, and with a dynamic response (including fast transients) that is very similar to that of the real converter.

Based on the above, it is concluded that the developed model is a powerful tool to predict the transient and steady-state response of the converter, obtain information on the effect of non-idealities on the dynamic response of the converter and evaluate the performance of different model-based control architectures.

Future work will focus on two different lines. First, the development of sensitivity analyses for characterization and isolatation, considering that they are present as coordinates of the state vector, and the influence of non-idealities according to the sizing and use of the converter (mainly power and operating frequency). Second, the design of more complete models that allow for the ripple in the output magnitudes of the converter to be modeled. Third, the design of optimal controllers to obtain the best possible converter performance.

Author Contributions: F.J.V.: writing—original draft, methodology, conceptualization, software, investigation, formal analysis, writing—review and editing. F.S.: writing—review and editing, conceptualization, methodology, funding acquisition. J.M.A.: writing—review and editing, conceptualization, supervision, project administration, funding acquisition. All authors have read and agreed to the published version of the manuscript.

Institutional Review Board Statement: Not applicable.

Informed Consent Statement: Not applicable.

Data Availability Statement: Not applicable.

Conflicts of Interest: The authors declare no conflict of interest.

References

1. Yuan, C.; Wan, J.; Zhou, H. Study on the dynamical characteristic for Voltage-feedback Push-Pull DC-DC converter. In Proceedings of the 2011 4th International Conference on Power Electronics Systems and Applications (PESA 2011), Hong Kong, China, 8–10 June 2011. [CrossRef]
2. Rahman, M.H.; Xu, L.; Yao, L. Protection of large partitioned MTDC Networks Using DC-DC converters and circuit breakers. *Prot. Control. Mod. Power Syst.* **2016**, *1*, 19. [CrossRef]
3. Li, Y.; Nejabatkhah, F. Overview of control, integration and energy management of microgrids. *J. Mod. Power Syst. Clean Energy* **2014**, *2*, 212–222. [CrossRef]
4. Cavallo, A.; Russo, A.; Canciello, G. Hierarchical control for generator and battery in the more electric aircraft. *Sci. China Inf. Sci.* **2019**, *62*, 192207. [CrossRef]
5. Enrique, J.M.; Dura, E. Theoretical assessment of the maximum power point tracking efficiency of photovoltaic facilities with different converter topologies. *Sol. Energy* **2007**, *81*, 31–38. [CrossRef]
6. Segura, F.; Andújar, J.M.; Durán, E. Analog current control techniques for power control in PEM fuel-cell hybrid systems: A critical review and a practical application. *IEEE Trans. Ind. Electron.* **2011**, *58*, 1171–1184. [CrossRef]
7. Trujillo, C.L.; Velasco, D.; Figueres, E.; Garcerá, G.; Ortega, R. Modeling and control of a push-pull converter for photovoltaic microinverters operating in island mode. *Appl. Energy* **2011**, *88*, 2824–2834. [CrossRef]
8. He, J.; Chen, K.; Li, M.; Luo, Y.; Liang, C.; Xu, Y. Review of protection and fault handling for a flexible DC grid. *Prot. Control. Mod. Power Syst.* **2020**, *5*, 15. [CrossRef]

9. Turksoy, A.; Teke, A.; Alkaya, A. A comprehensive overview of the dc-dc converter-based battery charge balancing methods in electric vehicles. *Renew. Sustain. Energy Rev.* **2020**, *133*, 110274. [CrossRef]

10. Kaya, M.; Costabeber, A.; Watson, A.; Tardelli, F.; Clare, J. A Push-Pull Series Connected Modular Multilevel Converter for HVdc Applications. *IEEE Trans. Power Electron.* **2022**, *37*, 3111–3129. [CrossRef]

11. Andújar, J.M.; Vivas, F.J.; Segura, F.; Calderón, A.J. Integration of air-cooled multi-stack polymer electrolyte fuel cell systems into renewable microgrids. *Int. J. Electr. Power Energy Syst.* **2022**, *142*, 108305. [CrossRef]

12. Delshad, M.; Farzanehfard, H. A new soft switched push pull current fed converter for fuel cell applications. *Energy Convers. Manag.* **2011**, *52*, 917–923. [CrossRef]

13. Liang, T.J.; Lee, J.H.; Chen, S.M.; Chen, J.F.; Yang, L.S. Novel isolated high-step-Up DC-DC converter with voltage lift. *IEEE Trans. Ind. Electron.* **2013**, *60*, 1483–1491. [CrossRef]

14. Ivanovic, Z.; Knezic, M. Modeling Push–Pull Converter for Efficiency Improvement. *Electronics* **2022**, *11*, 2713. [CrossRef]

15. Gómez, J.M.E.; Piña, A.J.B.; Aranda, E.D.; Márquez, J.M.A. Theoretical assessment of DC/DC power converters' basic topologies. A common static model. *Appl. Sci.* **2017**, *8*, 19. [CrossRef]

16. Davoudi, A.; Jatskevich, J.; De Rybel, T. Numerical state-space average-value modeling of PWM dc-dc converters operating in DCM and CCM. *IEEE Trans. Power Electron.* **2006**, *21*, 1003–1012. [CrossRef]

17. Garrigós, A.; Blanes, J.M.; Carrasco, J.A.; Lizán, J.L.; Beneito, R.; Molina, J.A. 5 kW DC/DC converter for hydrogen generation from photovoltaic sources. *Renew. Energy* **2010**, *35*, 6123–6130. [CrossRef]

18. Chen, Q.; Zheng, T.Q.; Li, Y.; Shao, T. The effect of transformer Leakage inductance on the steady state performance of push-pull based converter with continuous current. *J. Power Electron.* **2013**, *13*, 349–361. [CrossRef]

19. Qin, H.; Kimball, J.W. Generalized average modeling of dual active bridge DC-DC converter. *IEEE Trans. Power Electron.* **2012**, *27*, 2078–2084. [CrossRef]

20. Li, S.; Xiangli, K.; Smedley, K.M. A Control Map for a Bidirectional PWM Plus Phase-Shift-Modulated Push-Pull DC-DC Converter. *IEEE Trans. Ind. Electron.* **2017**, *64*, 8514–8524. [CrossRef]

21. Zhang, J.; He, Z.; Liu, Y.; Luo, A.; Wang, L.; Wang, H.; Chen, Y.; Pang, Y. High-Efficiency Push-Pull Resonant Converter Solution for Auxiliary Power Supply in 70-kV Isolated Applications. *IEEE J. Emerg. Sel. Top. Power Electron.* **2022**, *10*, 632–647. [CrossRef]

22. Zhang, H.; Quan, L.; Gao, Y. Dynamic modelling and small signal analysis of push-pull bidirectional DC-DC converter. *Comput. Model. New Technol.* **2014**, *18*, 14–18.

23. Larico, H.R.E.; Greff, D.S.; Heerdt, J.A. Modeling and control of a three-phase push-pull dc-dc converter: Theory and simulation. In Proceedings of the 2015 IEEE 13th Brazilian Power Electronics Conference and 1st Southern Power Electronics Conference, (COBEP/SPEC 2016), Fortaleza, Brazil, 29 November–2 December 2015; pp. 1–5. [CrossRef]

24. Cong, M.; Junfeng, W. Analysis and Modeling of a Voltage Compensated Push-pull DCX Converter. In Proceedings of the IEEE Information Technology, Networking, Electronic and Automation Control Conference (ITNEC 2021), Xi'an, China, 15–17 October 2021; pp. 489–493. [CrossRef]

25. Wu, J.J.; Sugimoto, H.; Wu, S.Y. Determination and relativity of the leakage inductance of push-pull transformers. In Proceedings of the PESC Record—IEEE Annual Power Electronics Specialists Conference, Jeju, Republic of Korea, 18–22 June 2006. [CrossRef]

26. Mumtaz, F.; Zaihar Yahaya, N.; Tanzim Meraj, S.; Singh, B.; Kannan, R.; Ibrahim, O. Review on non-isolated DC-DC converters and their control techniques for renewable energy applications. *Ain Shams Eng. J.* **2021**, *12*, 3747–3763. [CrossRef]

27. Hendra, A.; Hamada, F.; Yusivar, F. Voltage Control in Push-Pull DC-DC Converter using State Space Averaging PID with Soft-Start for Electric Vehicle Auxiliary System. In Proceedings of the 2019 6th International Conference on Instrumentation, Control, and Automation (ICA 2019), Bandung, Indonesia, 31 July–2 August 2019; pp. 188–193. [CrossRef]

28. Vivas, F.J.; Segura, F.; Andújar, J.M.; Caparrós, J.J. A suitable state-space model for renewable source-based microgrids with hydrogen as backup for the design of energy management systems. *Energy Convers. Manag.* **2020**, *219*, 113053. [CrossRef]

29. Vivas Fernández, F.J.; Manzano, F.S.; Márquez, J.M.A.; Calderón Godoy, A.J. Extended model predictive controller to develop energy management systems in renewable source-based smart microgrids with hydrogen as backup. Theoretical foundation and case study. *Sustainability* **2020**, *12*, 8969. [CrossRef]

30. Liu, X.; Wang, Y.; Zhu, J.; Guo, Y.; Lei, G.; Liu, C. Calculation of Capacitance in High-Frequency Transformer Windings. *IEEE Trans. Magn.* **2016**, *52*, 18–21. [CrossRef]

31. Tian, J.; Zhang, Y.; Ren, X.; Wang, X.; Tao, H. Calculation of Leakage Inductance of Integrated Magnetic Transformer with Separated Secondary Winding Used in ZVS PSFB Converter. *J. Magn.* **2016**, *21*, 644–651. [CrossRef]